

Zero-Voltage-Transition Buck Converter for High Step-Down DC–DC Conversion with Low EMI

Ali Ariyan* and Mohammad Rouhollah Yazdani†

*†Department of Electrical Engineering, Isfahan (Khorasgan) Branch, Islamic Azad University, Isfahan, Iran

Abstract

In this study, a new zero-voltage transition (ZVT) buck converter with coupled inductor using a synchronous rectifier and a lossless clamp circuit is proposed. The regular buck converter with tapped inductor has extended duty cycle for high step-down applications. However, the leakage inductance of the coupled inductor produced considerable voltage spikes across the switch. A lossless clamp circuit is used in the proposed converter to overcome this problem. The freewheeling diode was replaced with a synchronous rectifier to reduce conduction losses in the proposed converter. ZVT conditions at turn-on and turn-off instants were provided for the main switch. The synchronous rectifier switch turned on under zero-voltage switching, and the auxiliary switch turn-on and turn-off were under zero-current condition. Experimental results of a 100 W–100 kHz prototype are provided to justify the validity of the theoretical analysis. Moreover, the conducted electromagnetic interference of the proposed converter is measured and compared with its hard-switching counterpart.

Key words: Coupled inductor, Electromagnetic interference (EMI), High step-down converter, Synchronous rectifier, Zero-voltage transition (ZVT), Zero-current transition (ZCT)

I. INTRODUCTION

Currently, step-down or step-up voltage conversion is widely used in renewable energy conversion [1], [2]. Several applications, such as battery chargers and LED drivers, require high step-down voltage conversion [3], [4]. The buck topology is used for low-voltage and high-current applications [5]–[7]. However, limited duty cycle ratio, high switch stresses, high conduction, and switching losses make the regular buck converter an inappropriate solution for high step-down conversion. The tapped inductor is utilized to overcome the limited duty cycle ratio and achieve a high step-down or step-up conversion [8], [9]. However, the leakage inductance of the tapped inductor in the buck converter causes a high voltage spike across the switch, thereby increasing the switch voltage stress and electromagnetic interference (EMI). Lossless snubbers and clamp circuits can be used to mitigate the spike voltage created by the leakage inductance of tapped inductor [9]–[15].

In [10], the switch spike voltage is solved using a passive lossless snubber, which is proposed for a high step-up converter. Furthermore, switching loss is reduced, and diode reverse recovery is alleviated. In [16], an interleaved buck converter with an improved step-down conversion ratio using series capacitors is introduced. These modifications make this converter suitable for non-isolated applications that require high input voltage and low output current ripple. However, the maximum duty cycle is limited to 0.5, and the operation is under hard-switching condition. In addition, the voltage stress of input switch and diode reverse recovery problems exists. An interleaved buck converter is introduced in [17] with a high step-down conversion. However, two interleaved sections have four switches and four capacitors.

Considering that the operation under hard switching condition leads to high di/dt and dv/dt , which may cause to much EMI and switching losses, high step-down soft switching converters with coupled inductor are introduced [18]–[20]. Zero-voltage switching (ZVS) or zero-current switching (ZCS) can be achieved by adding an auxiliary cell. A soft-switched high step-down converter with a coupled inductor is introduced in [18]. In this converter, the switches turned on under ZVS condition. However, the turn-off of switches remained under hard-switching condition, and high-frequency voltage spikes occurred across the diodes,

Manuscript received Apr. 5, 2017, accepted Jul. 26, 2017
Recommended for publication by Associate Editor Yan Xing.

†Corresponding Author: mro.yazdani@gmail.com

Tel: +98-31-35354001, Fax: +98-31-35354060, Isfahan (Khorasgan) Branch, Islamic Azad University

*Department of Electrical Engineering, Isfahan (Khorasgan) Branch, Islamic Azad University, Iran

which can lead to high electromagnetic emissions. Moreover, the conduction losses of the freewheeling diode existed. A synchronous rectifier is used to decrease conduction loss combined with soft-switching techniques to solve the reverse recovery of freewheeling diode and improve the efficiency in low-voltage and high-current applications [21], [22]. In [22], a ZVS synchronous buck converter is proposed that can resolve the reverse recovery problem. The step-down conversion is not improved, and the turn-off of switches is under the hard-switching condition, although a coupled inductor is utilized in this converter. A critical-conduction mode (CRM) buck converter with a coupled inductor is proposed in [23]. The ZV condition at turn-on is instantly achieved for the switch, but the turn-off is under the hard-switching condition and high amplitude voltage spikes occur when the switch is turned off.

In this study, a high step-down converter using a coupled inductor, an auxiliary soft-switching cell, and a synchronous rectifier with a clamp circuit is introduced. The high step-down conversion is achieved using a coupled inductor. ZVT is provided for the main switch at turn-on and turn-off instants. The synchronous rectifier, where its switch is also turned on under ZV, is used to improve the efficiency. The turn-on and turn-off of the auxiliary switch are under zero-current transition. The lossless clamp is utilized to reduce switch voltage stress. In this study, EMI is another important issue considered in addition to high step-down conversion ratio and soft-switching condition evaluation, efficiency improvement, and voltage stress reduction.

The rest of this paper is organized as follows. Section II presents the theoretical analysis and operation intervals. Section III discusses the design considerations. Section IV describes the experimental waveforms and efficiency curves. Moreover, Section V presents the conducted EMI measurement results to show the benefit of the proposed converter in terms of electromagnetic compatibility. Section VI provides a comparison among high step-down ZV converters. Finally, Section VII summarizes the conclusion.

II. CIRCUIT DESCRIPTION AND OPERATION

The proposed soft-switching high step-down is shown in Fig. 1. Unidirectional auxiliary switch, S_a , and auxiliary inductor, L_a , compose the auxiliary soft-switching cell. The lossless clamp circuit consists of capacitor C_1 and two diodes, D_1 and D_2 . The following assumptions are considered to simplify the converter analysis.

- 1) Inductors, capacitors, and semiconductor components are ideal, and switch capacitances are disregarded.
- 2) The turn ratio of coupled inductor is $n = n_2/n_1$, and L_2 current is assumed constant and equal to output current I_O in a switching cycle.
- 3) C_1 is sufficiently large, and its voltage is nearly constant.

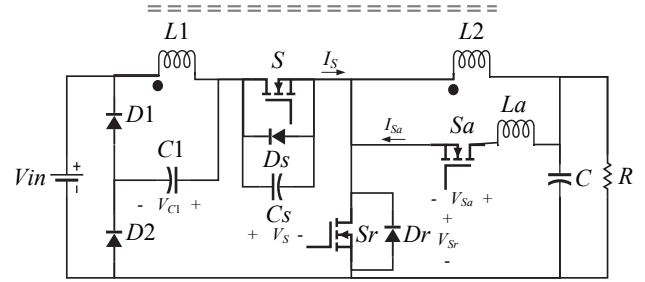


Fig. 1. Proposed soft-switching high step-down converter.

The equivalent circuit of each operating interval is presented in Fig. 2. Fig. 3 illustrates the theoretical waveforms of the proposed high step-down converter. Only the synchronous rectifier is on before the first interval, and other semiconductor devices are off.

Interval 1 [t_0-t_1], Fig. 2(a): At the beginning of this interval, the auxiliary switch turns on under ZCS because of the series auxiliary inductor. In this interval, output voltage V_o is placed across L_a ; thus, the current of the auxiliary inductor increases linearly to I_O . Furthermore, the current of synchronous rectifier decreases from I_O to zero. The L_a current and duration of this model are expressed as

$$I_{La} = \frac{V_o(t-t_0)}{L_a}, \quad (1)$$

$$t_1 - t_0 = \frac{I_O L_a}{V_o}. \quad (2)$$

At the end of this interval, the L_a current reaches I_O , and the current of S_r becomes zero.

Interval 2 [t_1-t_2], Fig. 2(b): In this interval, the synchronous rectifier remains on. Therefore, L_a current increases linearly from I_O to its maximum value and saves this extra energy to discharge the snubber capacitor in the next mode.

$$I_{La} = I_o + \frac{V_o(t-t_1)}{L_a} \quad (3)$$

$$t_2 - t_1 = \frac{(I_1 - I_o)L_a}{V_o} \quad (4)$$

At the end of this mode, L_a reaches its maximum current, which is defined as I_1 .

Interval 3 [t_2-t_3], Fig. 2(c): This interval starts by turning off S_r . In this interval, a resonance occurs between auxiliary inductor L_a and snubber capacitor C_s through the path of $C-L_a-S_a-C_s-C_1-D_1-V_{in}$. The current of leakage inductance traverses C_1 and D_1 . However, the voltage of C_1 remains constant because it is sufficiently large. Furthermore, the current of D_1 decreases to zero. Important equations of this mode are as follows:

$$I_{La} = I_o + \frac{V_o}{Z_o} \sin \omega_0(t-t_2) + (I_1 - I_o) \cos \omega_0(t-t_2), \quad (5)$$

$$V_{CS} = V_{in} + V_{C1} - V_o + V_o \cos \omega_0(t-t_2) - Z_o(I_1 - I_o) \sin \omega_0(t-t_2), \quad (6)$$

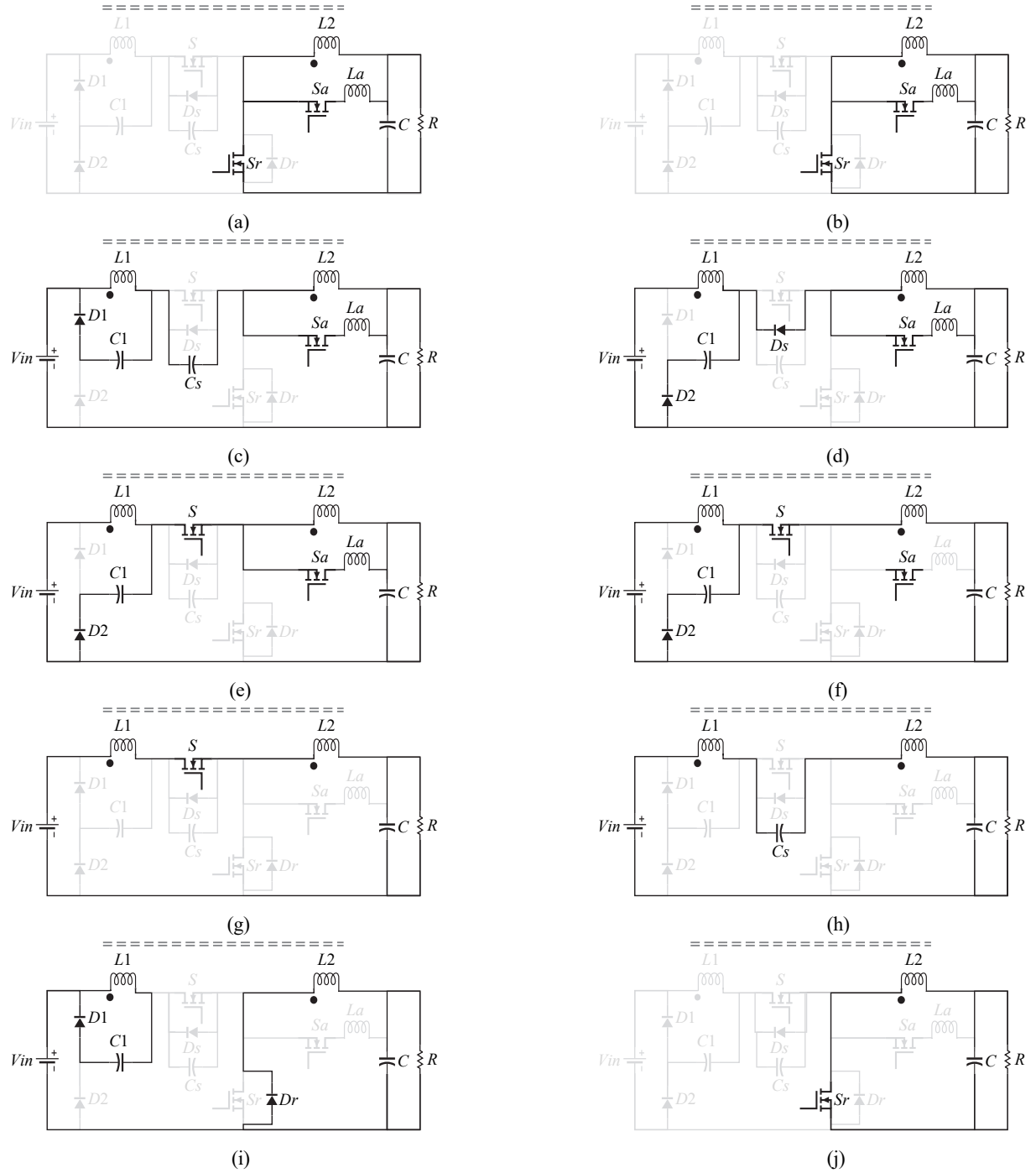


Fig. 2. Equivalent circuit for each operating interval. (a) $[t_0-t_1]$. (b) $[t_1-t_2]$. (c) $[t_2-t_3]$. (d) $[t_3-t_4]$. (e) $[t_4-t_5]$. (f) $[t_5-t_6]$. (g) $[t_6-t_7]$. (h) $[t_7-t_8]$. (i) $[t_8-t_9]$. (j) $[t_9-t_{10}]$.

Where

$$\omega_0 = \frac{1}{\sqrt{L_a C_s}}, \quad (7)$$

$$Z_0 = \sqrt{\frac{L_a}{C_s}}. \quad (8)$$

At the end of this interval, L_a current reaches I_2 that is greater than I_O , and C_s is discharged completely.

Interval 4 $[t_3-t_4]$, Fig. 2(d): In this interval, L_a continues its discharge. Thus, the body diode of the main switch starts to conduct. Therefore, snubber capacitor voltage becomes zero. Hence, the main switch is turned on under the ZV condition.

In this interval, D_2 starts to conduct. Thus, the capacitor of the clamp circuit discharges its extra energy. Important equations of this interval are expressed as follows:

$$I_{L_a} = I_2 - \frac{V_o - V_{C1}}{L_a} (t - t_3), \quad (9)$$

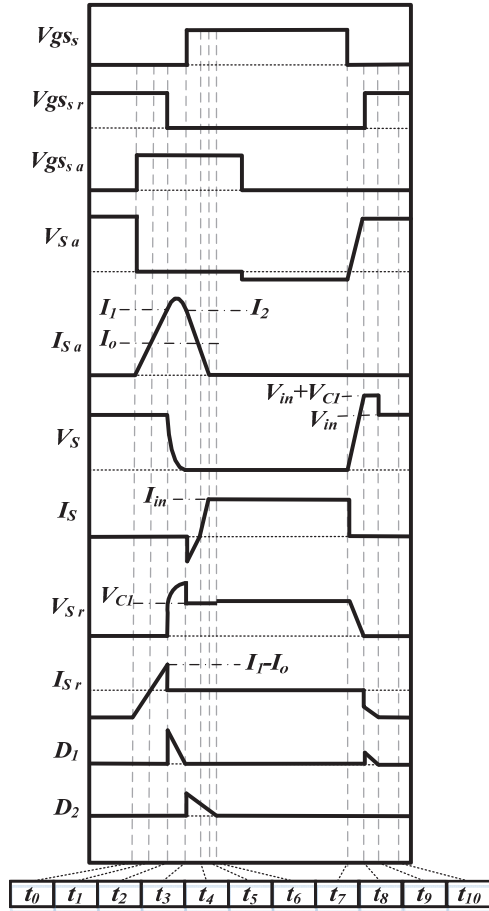


Fig. 3. Typical waveforms of the proposed converter.

$$t_4 - t_3 = L_a \frac{(I_2 - I_{La})}{V_o - V_{Cl}}. \quad (10)$$

At the end of this interval, L_a current decreases linearly to I_o , and the body diode of S is turned off.

Interval 5 [t_4-t_5], Fig. 2(e): The difference between the output and the capacitor of clamp circuit is placed across L_a given that main switch S is turned on. C_1 discharges its energy to the output through D_2 and L_2 . The equations of L_a current and duration of this interval are expressed as follows:

$$I_{La} = I_o - \frac{(V_o - V_{Cl})}{L_a} \cdot (t - t_4), \quad (11)$$

$$t_5 - t_4 = \frac{I_o - I_{La}}{V_o - V_{Cl}}. \quad (12)$$

At the end of this interval, the L_a current decreases linearly to zero, and I_s reaches I_{in} because the output and C_1 voltages are assumed constant in a switching cycle.

Interval 6 [t_5-t_6], Fig. 2(f): In this interval, main switch S remains on, and C_1 is discharged. At the end of this interval, V_{Cl} reaches its initial value, and D_2 is turned off. The equation of V_{Cl} at the end of this mode is expressed as follows.

$$V_{Cl} \approx \frac{nV_{in} + V_o}{n + 1} \quad (13)$$

Interval 7 [t_6-t_7], Fig. 2(g): L_1 and L_2 absorb the power from the input because the main switch is on, and the input energy is transmitted to the output. L_a current is zero. Thus, the auxiliary switch can be turned off under ZCS. Considering L_t as the total inductance of series coupled inductances L_1 and L_2 , the current of L_1 and the duration of this mode are expressed as:

$$I_{L1} = \frac{(V_{in} - V_o)}{L_t} \cdot (t - t_6), \quad (14)$$

$$t_7 - t_6 = \frac{I_{L1} \cdot L_t}{V_{in} - V_o}. \quad (15)$$

Interval 8 [t_7-t_8], Fig. 2(h): In this interval, the main switch is turned off under the ZV condition because of the existence of snubber capacitance. Accordingly, C_s is charged, and its voltage reaches $V_{in} + V_{Cl}$.

Interval 9 [t_8-t_9], Fig. 2(i): At the beginning of this interval, S_r body diode and D_1 start to conduct. Hence, the synchronous switch can be turned on under the ZV condition. The energy of L_1 is stored in C_1 , and its current reduces linearly. The stress voltage of the main switch is clamped by the clamp capacitor. The current of L_2 and S_r body diode increases linearly. At the end of this interval, the current of L_1 becomes zero, and the current of S_r body diode and L_2 reaches I_o .

Interval 10 [t_9-t_{10}], Fig. 2(j): In this interval, the output current flows through S_r and L_2 . This mode continues until the gate pulse of S_a is applied, and the next cycle of switching is started.

III. DESIGN CONSIDERATION

The proposed converter is designed for 150 V input voltage, 24 V output voltage, and 100 W output power at 100 kHz switching frequency. The conversion gain is obtained using the L_1 volt-second balance, which is expressed by:

$$\frac{V_o}{V_{in}} = \frac{D}{1 + \frac{1}{n}(1-D)}, \quad (16)$$

where n is n_2/n_1 . Fig. 4 depicts the curves of voltage gain versus the duty cycle of the proposed converter for various turn ratio n .

The total inductance of series coupled inductor L_t , which is equal to $(1+1/n)^2$. L_2 can be calculated similarly to a regular buck converter. Thus, L_2 can be written as

$$L_2 = \frac{(V_i - V_o)D}{(1 + \frac{1}{n})^2 f_{sw} \Delta i_L}. \quad (17)$$

The relationship between L_2 and L_1 is determined by the turn-ratio of the magnetic element.

$$\frac{L_2}{L_1} = \left(\frac{n_2}{n_1}\right)^2 = n^2 \quad (18)$$

For a given gain, the values of L_1 and L_2 are determined according to (17) and (18), as summarized in Table I, for

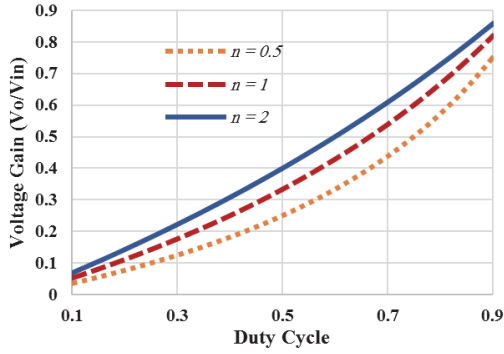


Fig. 4. Gain voltage of the proposed converter for various n .

$n = 1$. Low output voltage leads to a low value of n . In this case, the L_1 value can be increased to avoid a minimal value of L_2 , which indicates that inductor current ripple Δi_L is not increased according to (17).

The design of snubber capacitor C_s is similar to other regular turn-off snubber capacitors [24].

$$C_{s_{\min}} = \frac{I_{SW} \cdot t_f}{2 \cdot V_{SW}} \quad (19)$$

where I_{SW} is the switch current before turn off, V_{SW} is the voltage after turn off, and t_f is the switch current fall time. C_s is selected with a larger value than $C_{s_{\min}}$ to ensure the soft-switching condition.

The value of L_a is similar to a regular turn-on snubber inductor [24], which should satisfy the following relation to guarantee the soft-switching condition:

$$\frac{1}{2} \cdot L_a \cdot (I_1 - I_o)^2 \geq \frac{1}{2} \cdot C_s \cdot (V_{in} + V_{C1})^2 \quad (20)$$

The control circuit is designed similar to its hard-switching counterpart through a PWM controller. The scheme depicted in Fig. 5 is used to achieve the required timings for each switch pulse and adjust the PWM controller pulse for three switches. The soft-switching condition is provided from minimum to full load similar to other soft-transition converters because delay times are fixed for the worst case.

IV. EXPERIMENTAL WAVEFORMS AND EFFICIENCY

A 100 W, 150–24 V prototype of the proposed converter at 100 kHz switching frequency is constructed to verify the theoretical analysis and key waveforms. The passive component values are listed in Table I. IRF740 is selected for the main switch, S and IRF640 are utilized for S_a and S_r , S_a contains a series diode to act as a unidirectional auxiliary switch. D16S60C is used for diodes. The photo of the prototype is depicted in Fig. 6 The voltage and current waveforms are measured using Tektronix TDS2014c oscilloscope and PINTEK PA-677 current probe. Fig. 7 displays the voltage and current waveforms of the main switch and its turn-on and turn-off instants, which confirm the ZVT

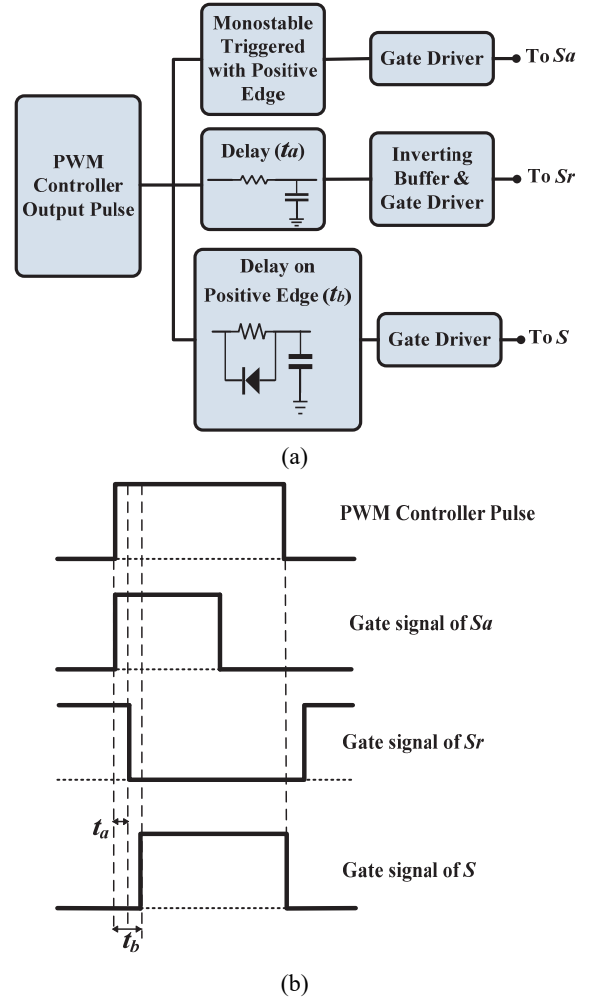


Fig. 5. (a) Driver circuit, (b) Timing diagram.

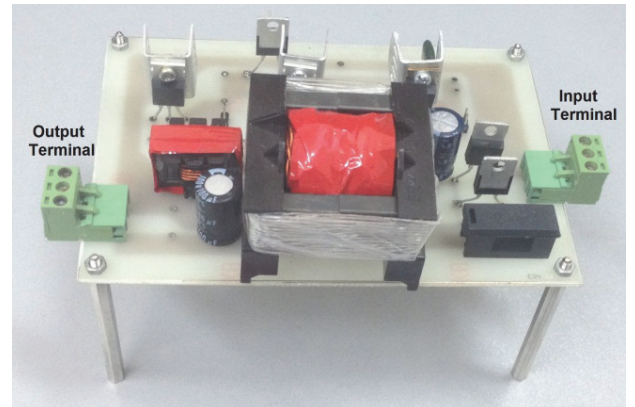


Fig. 6. Photo of the proposed converter prototype.

TABLE I
COMPONENT VALUES OF THE PROTOTYPE

Component	Value
L_1, L_2	300 μH
C_1	10 μF
C_s	2.2 nF
C	100 μF
L_a	3 μH

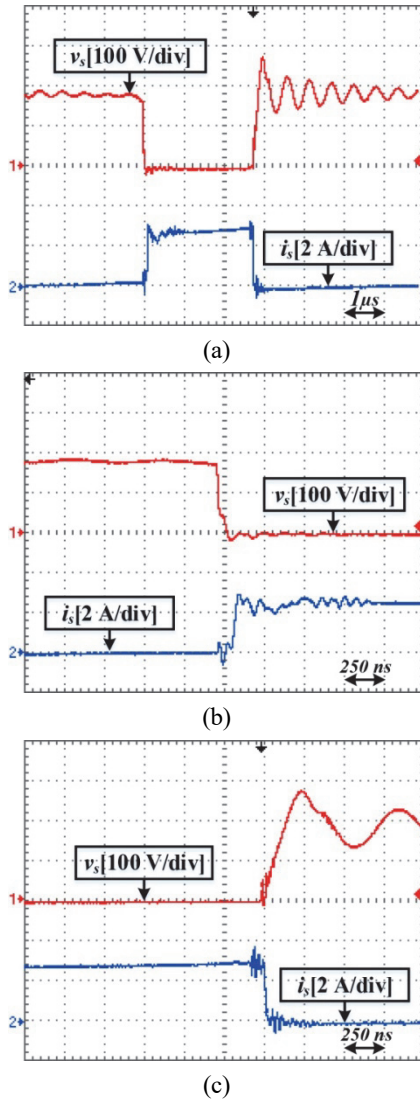


Fig. 7. (a) Voltage (top) and current (bottom) waveforms of the main switch, (b) turn-on instant, (c) turn-off instant.

operation of the main switch.

In Fig. 7 (b), the body diode of the main switch is conducted before the switch turn on. The snubber capacitor provides the ZV condition for turning off, as demonstrated in Fig. 7 (c). In Fig. 7, the voltage spike caused by the leakage inductance of the coupled inductor is clamped by the clamp circuit. Fig. 8 (a) displays the ZCS operation of the auxiliary switch. The auxiliary switch turns on and off under ZCS. The voltage and current of synchronous switch S_r is illustrated in Fig. 8 (b). S_r turn on is under ZV, as discussed in the theoretical analysis. Furthermore, the current waveforms of D_1 and D_2 are shown in Figs. 9 (a) and (b), correspondingly.

The semiconductor device losses of the prototype are tabulated in Table II. Fig. 10 illustrates the efficiency curve of the proposed converter and hard-switching buck converter with a tapped inductor. A unidirectional switch can be used rather than series diode (D_a) and S_a to reduce the conduction loss caused by this series diode.

TABLE II
SEMICONDUCTOR LOSSES IN THE PROPOSED CONVERTER

Type of loss	Element	Loss (W)
Conduction losses of switches (W) $R_{ds} \cdot f_{sw} \cdot \int I_s^2 dt$	S	0.9
	S_a	2.1
	S_r	3.12
Capacitive losses of switches (W) $\frac{1}{2} C_o V_{ds}^2 f_{sw}$	S	0.08
	S_a	0.05
	S_r	0.075
Conduction losses of diodes (W) $I_{ave} \cdot V_F$	D_1	0.005
	D_2	0.01
	D_a	1.2

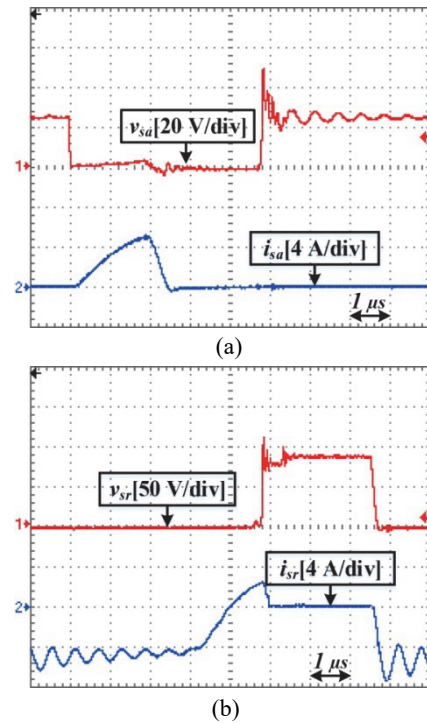


Fig. 8. Experimental voltage and current waveforms: a) S_a , b) S_r .

V. CONDUCTED EMI MEASUREMENT

In this section, the experimental measurement of conducted EMI for the proposed converter and its hard-switching counterpart with a tapped inductor is evaluated. Conducted electromagnetic emissions are measured according to the CISPR 22 standard. CISPR 22 line impedance stabilization network (LISN) is inserted between the converters and input lines. The measured conducted EMI for the hard-switching buck converter with a tapped inductor and the proposed converter are displayed in Figs. 11(a) and 10(b), respectively, using GW-Instek GSP830 spectrum analyzer. In Fig. 11, the main conducted EMI peak for the hard-switching buck and proposed converters are approximately 91 and 84 dB μ V, respectively, indicating that the main peak of the proposed converter is reduced in terms of its hard-switching counterpart

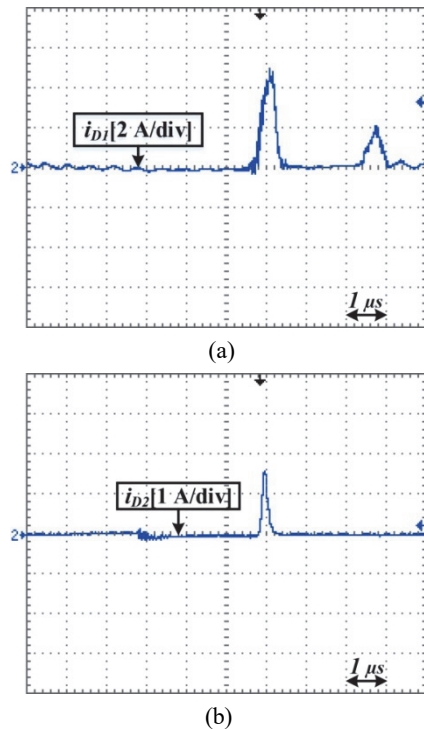


Fig. 9. Experimental result waveforms: a) D_1 current, b) D_2 current.

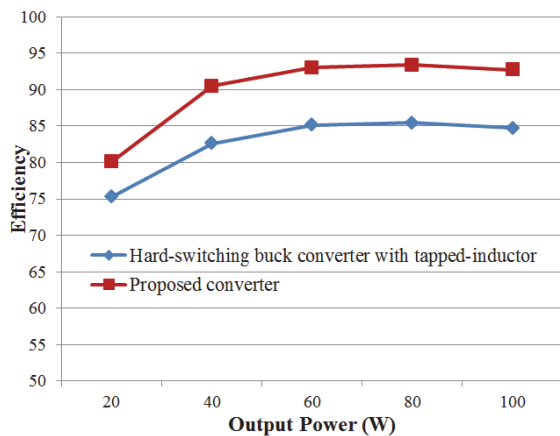


Fig. 10. Efficiency curves of the proposed converter and hard-switching buck converter with tapped inductor.

by providing soft-switching and clamp techniques. For further EMI comparison, Fig. 12 compares EMI peaks in various frequency bands. According to CISPR 22 Class A limit (79 dB μ V for 0.15–0.5 MHz and 73 dB μ V for 0.5–30 MHz frequency band), the EMI levels of the proposed converter are under the standard limit (73 dB μ V) at approximately 13–30 MHz frequency band, whereas its hard-switching converter has an EMI level higher than the standard limit in most frequency bands. The proposed converter contains several frequencies below 13 MHz with higher values than CISPR 22. An EMI filter with low characteristics and attenuation can be used for 0.15–13 MHz to satisfy CISPR 22 at this frequency band because the emission levels are significantly reduced in the

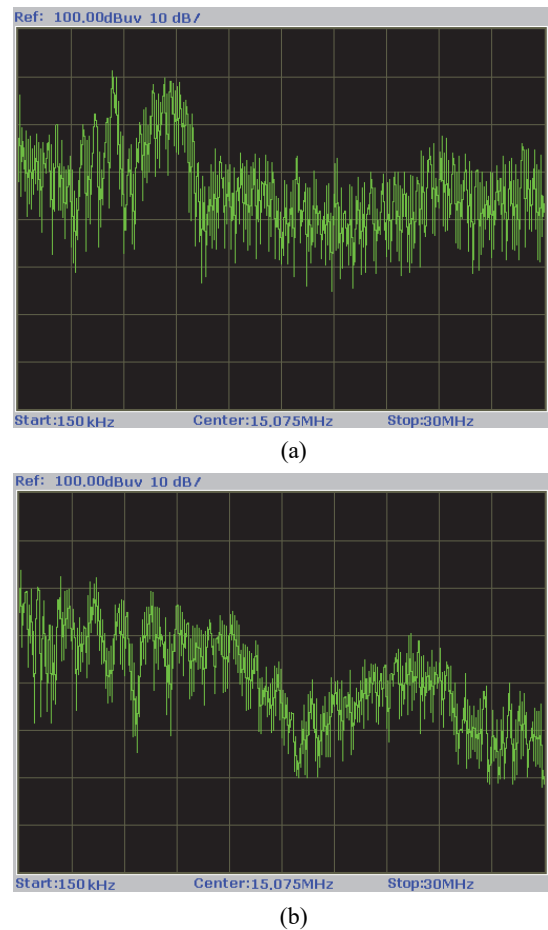


Fig. 11. Conducted EMI measurement of a) hard-switching buck converter with tapped inductor b) proposed converter (Ver. axis: 20–100 dB μ V, Hor. axis: 0.15–30 MHz).

proposed converter with respect to its hard-switching counterpart.

VI. COMPARISON WITH OTHER HIGH STEP-DOWN ZV CONVERTERS

A comparison between the proposed and another ZVS high step-down converters is presented in Table III. All converters are designed with components and specifications similar to the proposed converter. In addition to efficiency at nominal load, the conducted EMI of converters and the proposed converter is simulated using LISN and the converter circuit model in OrCAD. Instead of the measured EMI peak value, The simulated EMI peak value of the proposed converter is shown, rather than its measured EMI peak, because the EMI of [18], [20], and [25] are simulated value. The converter in [25] can only operate in the CRM and has a limitation for soft-switching operation area versus load range, although it had fewer components than other converters. Similar to other soft-transition converters, the soft-switching condition is independent of load changes in the proposed converter compared with regular resonant converters. In [20],

TABLE III
COMPARISON OF HIGH STEP-DOWN ZERO-VOLTAGE CONVERTERS ($V_{IN}=150\text{ V}$, $V_O=24\text{ V}$, $P_O=100\text{ W}$)

Converter	Efficiency (%)	EMI Peak (dB μ V)	Number and Value of Elements				Switching condition					
			Switch	Diode	Magnetic Core	Capacitor	Main switch		Another switch		Synchronous switch	
							ON	OFF	ON	OFF	ON	OFF
[18]	89	90.5	2	2	No.: 2 Coupled Inductor Small Inductor (<10 μ H)	No.: 3 10 μ F, 50 μ F, 2400 μ F	ZV	Hard	ZV	Hard	Without Sync. Switch	
[20]	88.5	96.7	3	0	No.: 2 Coupled Inductor Large Output Inductor	No.: 3 20 μ F, 40 μ F, 660 μ F	ZV	Hard	ZV	Hard	Nearly ZV	Hard
[25]	91.3	93.1	2	0	No.: 1 Coupled Inductor	No.: 1 100 μ F	ZV	Hard	Without Aux. Switch		ZV	Hard
This Work	92.5	87	3	2	No.: 2 Coupled Inductor Small Inductor (<10 μ H)	No.: 3 2.2 nF, 10 μ F, 100 μ F	ZV	ZV	ZC	ZC	ZV	Hard

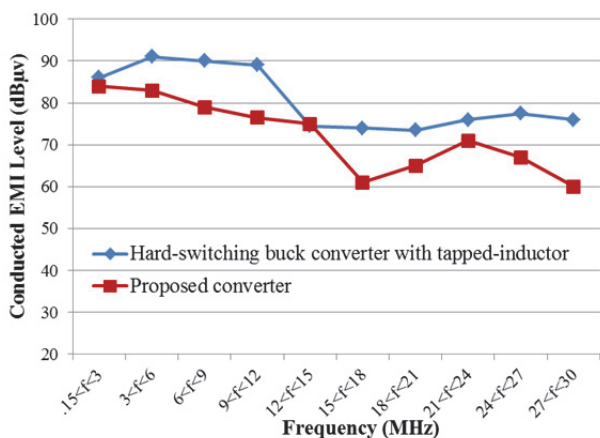


Fig. 12. Comparison of conducted EMI peaks in various frequency bands – experimental results.

high-frequency spikes occur across the synchronous switch caused by leakage inductance, yielding much EMI, which is confirmed by a simulated EMI peak. In addition to enhanced efficiency, the EMI simulation shows that the proposed converter has lower EMI peak due to better soft-switching conditions at switching instants over the abovementioned converters.

VII. CONCLUSIONS

In this study, a soft-switching high step-down converter with an auxiliary cell, a lossless clamp circuit, and a synchronous rectifier where its duty cycle is extended by a coupled inductor is proposed. The theoretical and experimental results indicate that the main switch turns on and off under the ZV condition. The turn-on of the synchronous switch is ZV, and the auxiliary switch turn-on and turn-off are under ZC. A lossless clamp limits the voltage spike of the main switch generated by leakage inductance in buck converters with a coupled inductor and recovers its energy. The efficiency of the proposed

converter is improved compared with the hard-switching buck converter with a tapped inductor and other similar ZV converters. Furthermore the proposed converter exhibited a lower EMI peak than the hard-switching and three similar ZV converters.

REFERENCES

- [1] H. Wu, K. Sun, R. Chen, H. Hu, and Y. Xing, "Full-Bridge three-port converters with wide input voltage range for renewable power systems," *IEEE Trans. Power Electron.*, Vol. 27, No. 9, pp. 3965-3974, Sep. 2012.
- [2] Y. Zhang, J. Liu, X. Ma, and J. Feng, "Comparison of conventional DC-DC converter and a family of diode-assisted DC-DC converter in renewable energy applications," *Journal of Power Electronics*, Vol. 14, No. 2, pp. 203-216, Mar. 2014.
- [3] L. Chen, H. Wu, Y. Xing, and X. Xiao, "Performance evaluation of a 1kW non-isolated high step-up/step-down bidirectional converter for distributed battery storage system," in *2015 IEEE 2nd International Future Energy Electronics Conference (IFEEEC)*, pp. 1-5, 2015.
- [4] Q. Luo, B. Zhu, W. Lu, and L. Zhou, "High step-down multiple-output LED driver with the current auto-balance characteristic," *Journal of Power Electronics*, Vol. 12, No. 4, pp.519-527, Jul. 2012.
- [5] H. Sira-Ramirez and M. A. Oliver-Salazar, "On the robust control of buck-converter DC-motor combinations," *IEEE Trans. Power Electron.*, Vol. 28, No. 8, pp. 3912-3922, Aug. 2013.
- [6] M. G. Kim, "Error amplifier design of peak current controlled (PCC) buck LED driver," *IEEE Trans. Power Electron.*, Vol. 29, No. 12, pp. 6789-6795, Dec. 2014.
- [7] A. De Nardo, N. Femia, G. Petrone, and G. Spagnuolo, "Optimal buck converter output filter design for point-of-load applications," *IEEE Trans. Ind. Electron.*, Vol. 57, No. 4, pp. 1330-1341, Apr. 2010.
- [8] T. Modeer, S. Norrga, and H. P. Nee, "High-voltage tapped-Inductor buck converter utilizing an autonomous high-side switch," *IEEE Trans. Ind. Electron.*, Vol. 62, No. 5, pp. 2868-2878, May. 2015.
- [9] K. Yao, M. Ye, M. Xu, and F. C. Lee, "Tapped-inductor

- buck converter for high-step-down DC-DC conversion," *IEEE Trans. Power Electron.*, Vol. 20, No. 4, pp. 775-780, Jul. 2005.
- [10] J.-il Kang, S.-K. Han, and J. Han, "Lossless snubber with minimum voltage stress for continuous current mode tapped-inductor boost converters for high step-up applications," *Journal of Power Electronics*, Vol. 14, No. 4, pp. 621-631, Jul. 2014.
- [11] D.-H. Jang, J.-I. Kang, and S.-K. Han, "High efficiency lossless snubber for photovoltaic maximum power point tracker," *Trans. the Korean Institute of Power Electronics (KIPE)*, Vol. 18, No. 5, pp. 485-491, Oct. 2013.
- [12] M. Nakamura, K. Ogura, and M. Nakaoka, "Soft switching PWM boost chopper-fed dc-dc power converter with load side auxiliary passive resonant snubber," *Journal of Power Electronics*, Vol. 4, No. 3, pp. 161-168, Jul. 2004.
- [13] T. Ahmed, S. Nagai, E. Hiraki, and M. Nakaoka, "A new three winding coupled inductor-assisted high frequency boost chopper type dc-dc power converter with a high voltage conversion ratio," *Journal of Power Electronics*, Vol. 5, No. 2, pp. 99-103, Apr. 2005.
- [14] J.-M. Kang, S.-H. Lee, S.-S. Hong, and S.-K. Han, "Voltage clamped tapped-inductor boost converter with high voltage conversion ratio," *Trans. the Korean Institute of Power Electronics (KIPE)*, Vol. 17, No. 1, pp. 34-40, Feb. 2012.
- [15] J. J. Yun, H. J. Choe, Y. H. Hwang, Y. K. Park, and B. Kang, "Improvement of power-conversion efficiency of a DC–DC boost converter using a passive snubber circuit," *IEEE Trans. Ind. Electron.*, Vol. 59, No. 4, pp. 1808-1814, April 2012.
- [16] I. O. Lee, S. Y. Cho, and G. W. Moon, "Interleaved buck converter having low switching losses and improved step-down conversion ratio," *IEEE Trans. Power Electron.*, Vol. 27, No. 8, pp. 3664-3675, Aug. 2012.
- [17] C.-T. Pan, C.-F. Chuang, and C.-C. Chu, "A novel transformerless interleaved high step-down conversion ratio dc–dc converter with low switch voltage stress," *IEEE Trans. Ind. Electron.*, Vol. 61, No. 10, pp. 5290–5299, Oct. 2014.
- [18] R. J. Wai and J. J. Liaw, "High-efficiency coupled-inductor-based step-down converter," *IEEE Trans. Power Electron.*, Vol. 31, No. 6, pp. 4265-4279, Jun. 2016.
- [19] C. T. Tsai, C. L. Shen, J. C. Su, and Y. C. Kuo, "Analysis and implementation of an interleaved ZVS buck converter with coupled-inductors," in *2011 6th IEEE Conference on Industrial Electronics and Applications*, pp. 1392-1397, 2011.
- [20] K. I. Hwu, W. Z. Jiang, and Y. T. Yau, "Nonisolated coupled-inductor-based high step-down converter with zero DC magnetizing inductance current and non-pulsating output current," *IEEE Trans. Power Electron.*, Vol. 31, No. 6, pp. 4362-4377, Jun. 2016.
- [21] E. Adib and H. Farzanehfard, "Zero-voltage-transition PWM converters with synchronous rectifier," *IEEE Trans. Power Electron.*, Vol. 25, No. 1, pp. 105-110, Jan. 2010.
- [22] H. L. Do, "Zero-voltage-switching synchronous buck converter with a coupled inductor," *IEEE Trans. Ind. Electron.*, Vol. 58, No. 8, pp. 3440-3447, Aug. 2011.
- [23] J.-H. Park and B.-H. Cho, "The zero voltage switching (ZVS) critical conduction mode (CRM) buck converter with tapped-inductor," *IEEE Trans. Power Electron.*, Vol. 20, No. 4, pp. 762–774, Jul. 2005.
- [24] N. Mohan, T. M. Undeland, W. P. Robbins, *Power Electronics*, 3rd ed., New York: Wiley, 2003.
- [25] J. H. Park and B. H. Cho, "Nonisolation soft-switching buck converter with tapped-inductor for wide-input extreme step-down applications," *IEEE Trans. Circuits and Systems I: Regular Papers*, Vol. 54, No. 8, pp. 1809-1818, Aug. 2007.



interests include soft-switching power converters and EMI.

Ali Ariyan was born in Isfahan, Iran, in 1989. He received his B.S. and M.S. degrees in Electrical Engineering from Najafabad and Isfahan (Khorasgan) Branches, Islamic Azad University in 2013 and 2016, respectively. Since 2016, he has been a member of the Young Researchers and Elite Club of Islamic Azad University. His current research



interests include soft-switching power converters and EMI.

Mohammad Rouhollah Yazdani was born in Isfahan, Iran in 1978. He received his B.S., M.S., and Ph.D. degrees in Electrical Engineering from the Isfahan University of Technology, Najafabad Branch, Islamic Azad University, and Sciences & Research Branch, Islamic Azad University in 2001, 2004, and 2011, respectively. Since 2011, he has been a Faculty Member at the Department of Electrical and Computer Engineering, Isfahan (Khorasgan) Branch, Islamic Azad University, Isfahan, Iran. His research interests include soft-switching converters, EMI reduction techniques, signal integrity, and EMC issues.